PUBLICATIONS OF THE ASTRONOMICAL SOCIETY OF THE PACIFIC, **122**:1471–1482, 2010 December

Polarization Gratings: A Novel Polarimetric Component for Astronomical Instruments

C. PACKHAM,[1] M. ESCUTI,[2] J. GINN,[3] C. OH,[2] I. QUIJANO,[3] AND G. BOREMAN[3]

Received 2010 March 12; accepted 2010 October 18; published 2010 November 18

Polarization gratings (PGs) have been recently been developed for ultraefficient liquid crystal displays, nonmechanical optical beam steering, and telecommunication devices at optical and near-infrared wavelengths (0.4–2.0 μm). A PG simultaneously acts as both a spectroscopic and polarimetric disperser for circularly polarized light. With the use of a quarter-wave retarder (or analog) to convert linearly to circularly polarized light, these devices can be used as linear polarimetric analyzers. PGs offer high throughput and high levels of birefringence and can currently be constructed inexpensively to diameters of 150 mm, and development projects are in progress to double that size. In this article we report on the characterization of a PG sample at mid-infrared wavelengths (2–40 μm), including the birefringence, throughput, spectral response, and cold cycling survivability. We discuss these devices in the context of astronomical polarimetry, especially as the polarimetric components for a conceptual study of a SOFIA-based polarimeter.

Online material: color figures

1. INTRODUCTION

Polarimeters are deployed on several of the world's large telescopes, both at nighttime and solar observatories. Among the large nighttime telescopes, most have provision for polarimetry (currently or in the near future) in at least one component of their regularly available instrumentation suites. Demand for polarimeters on such telescopes remains a small but significant fraction of the total time requested; in the case of Michelle (the 7–25 μm imager, spectrometer, and polarimeter on the 8.1 m Gemini North (Glasse et al. 1997), immediately after commissioning of the polarimetry mode, demand for polarimetry peaked at 20% of the total Michelle time requested (taken from the Gemini World Wide Web pages[4]). Perhaps a more appropriate comparison (due to the longer baseline of usage statistics) is provided through comparison with the ISIS (Intermediate-dispersion Spectrograph and Imaging System) polarimetry mode on the 4.2 m William Herschel Telescope (WHT). ISIS is a dual-arm (blue and red) optical spectrograph, commissioned in 1989, and polarimetry was offered one year later. Demand for ISIS has remained consistently high since commissioning, and the instrument quickly became, and still is, the most requested instrument on the WHT. Between 2003 February and 2007 July, polarimetry on ISIS enjoyed an average demand of 9% of all awarded ISIS time, with a peak semester demand of 24% (I. Skillen 2008, private communication), representing a healthy demand for polarimetry. Astronomical applications of polarimetry are many and varied, including observations of debris disks around stars (Tamura et al. 2006), young stellar objects (Chrysostomou et al. 1996), ultracool dwarfs (Tata et al. 2009), and key optical observations in unified theories of active galactic nuclei (AGNs; Antonucci et al. 1985) and supported by Gemini polarimetry at 10 μm (Packham et al. 2007).

Advances in telescope design and instrumentation have greatly benefited users, but these advances can have detrimental effects on polarimetry. The development of adaptive optics (AO) on telescopes (e.g., WHT [Myers et al. 2003], VLT [Rousset et al. 2003], Keck [Wizinowich et al. 2000], and Gemini [Rigaut et al. (2000]) can increase the spatial resolution by over an order of magnitude through the reduction or elimination of the blurring effects of the Earth's atmosphere. This is accomplished through using typically complex and convoluted optical systems, including deformable mirrors, dichroic components, and oblique reflections. While an increase in spatial resolution often leads to a higher *measured* degree of polarization (otherwise reduced due to an averaging of the polarization in unresolved sources that do not have a single position angle of polarization), at optical wavelengths a freshly coated and dust-free aluminum 45° flat mirror introduces a polarization of ~10% (Leroy 2000) or ~0.8% at K (2.2 μm) (using data from Gray 1963, p. 6), and a succession of flat and dichroic components can introduce crosstalk between linear and circular

[1] Department of Astronomy, University of Florida, 211 Bryant Space Science Center, Gainesville, FL 32611; packham@astro.ufl.edu.

[2] Department of Electrical and Computer Engineering, North Carolina State University, 2410 Campus Shore Drive, Raleigh, NC 27695.

[3] Center for Research and Education in Optics and Lasers, The College of Optics and Photonics, University of Central Florida, 4000 Central Florida Boulevard, Orlando, FL 32816.

[4] See http://www.gemini.edu.

polarizations. Changes in the cleanliness and coating performance of mirrors have a significant effect on the instrumental polarization, and hence AO systems typically contribute a significant level of, and often temporally variable, instrumental polarization. This can frustrate polarimetric observations, especially when an object's degree of polarization is similar to or less than that of the instrumental polarization. The advent of AO secondary mirrors, such as that pioneered at the 6.5 m MMT (Brusa et al. 2003), offers the chance to observe at the diffraction limit of large telescopes but with negligible increased instrumental polarization. Although developed primarily to reduce the thermal background from the telescope for MIR work, the MMT's AO secondary has the added advantage that there are *no* off-axis reflections, making it ideal for high-precision polarimetry in the 1–5 μm regime. A National Science Foundation (NSF)-funded polarimeter is currently under construction using the traditional and commonly implemented methodology of a crystalline half-wave retarder and Wollaston prism to offer dual-beam polarimetry (Packham & Jones 2008).

Despite these problems, AO-optimized polarimeters have been deployed on large telescopes, especially when the absolute value of polarization is less important (Perrin et al. 2008). The next generation of large telescopes (such as the 30 m class of observatories) with adaptive optics system integral to their design will likely have a complex optical design and possibly no provision for a Cassegrain focus. For AO polarimetry, it is best to modulate the beam before the AO optics, but the beam size is often large before input to the AO system, and 30 m class instruments will likely have large pupils interior to the cryostat. Even if AO is not used, the common use of the unfolded Cassegrain focus of telescopes by IR instruments means that this focal station is often occupied, potentially requiring the use of other folded focal stations for polarimeters, also leading to increased instrumental polarization. The factors discussed previously lead to the requirements of large modulation and analyzer optics, increasing costs and production time, and possibly requiring components of a size beyond that which can currently be produced.

Although there are several dual-beam polarimeters available on large telescopes that cover the 1–5 μm wavelength region, few are available at longer wavelengths. The CanariCam instrument (Packham et al. 2005) has a dual-beam polarimeter that will offer diffraction-limited polarimetry ($\sim$0.3″) between 7.5 and 13.5 μm (the N-band atmospheric window). The modulator (a half-wave retarder, 33 mm diameter) and analyzer (a Wollaston prism, 38×33 mm) are constructed from antireflection coated sulfur-free cadmium selenide (CdSe), optimized for use at 10.5 μm. The Wollaston prism, the largest currently available, has a throughput of $\geq$70% between 7 and 13 μm and $\geq \sim 20\%$ up to $\sim$23 μm (Packham et al. 2008). However, at wavelengths beyond 23 μm the transmission falls to zero. Should one require either polarimetric observations at $> \sim 23$ μm or large polarimetry optics, crystalline materials currently do not offer a viable solution.

NASA's 2.5 m airborne telescope, the Stratospheric Observatory for Infrared Astronomy (SOFIA), is expected to enter regular operation in 2011, and second-generation instrument concepts will soon be solicited. In preparation for this opportunity, we recently engaged in a design study for a mid-infrared (MIR; 5–40 μm) polarimeter for the observatory (Packham et al. 2008). As the science enabled for such a polarimeter is unique and exciting, such as observations of the cooler outer regions of debris disks, astrochemistry, and AGN (discussed in Packham et al.2007), but neither crystalline materials nor traditionally used materials/techniques for a dual-beam polarimeter are available for use at these wavelengths, we investigated the properties of PGs at these wavelengths.

In this article we discuss the characterization of a 5–40 μm optimized PG and discuss the applicability to astronomical instrumentation. In § 2 we introduce PGs and their physical structure, and in § 3 we discuss the measurement techniques. In § 4 we discuss measured liquid crystal polymer (LCP) birefringence, throughput, and narrowband PG polarization and diffraction behavior. In § 5 we discuss broadband PG for the MIR operation, estimate the performance of current and improved materials, and report cold survivability. Finally, in § 6 we conclude and summarize our results.

2. POLARIZATION GRATINGS

A novel polarizing beamsplitter using birefringent gratings (Oh & Escuti 2007a, 2008; Escuti et al. 2006) is being pioneered at North Carolina State University (NCSU). The key optical element is called a polarization grating (Crawford et al. 2005; Nersisyan et al. 2009; Gori 1999; Nikolova & Todorov 1984; Tervo & Turunen 2000), which is a thin-film beamsplitter that is functionally analogous to a Wollaston prism (see Figs. 1a–1c). In both elements, incident light is angularly separated into two forward-propagating orthogonal polarizations; however, PGs employ the Pancharatnam-Berry phase-delay (McManamon et al. 2009) principle and operate on circular eigenpolarizations, whereas Wollaston prisms employ the double-refraction effect and operate on linear eigenpolarizations. As implemented within this work, the PG beamsplitter is made up of a thin polymer film (less than 300 μm thick) comprising a LCP coated optionally on a reflective or transparent substrate and can be made with almost any surface area. The essential structure of these polarization gratings is implemented using uniaxially birefringent, polymerizable, liquid crystal materials (Kelly 1995), arranged into a continuous, in-plane, bend-splay pattern (an example of which is shown in Fig. 1d). This pattern is established using a UV polarization hologram exposing photoalignment materials (Escuti et al. 2006; Schadt et al. 1996), followed by spin-coating of the polymerizable liquid crystal.

The polarization behavior and diffraction efficiency spectra of this PG are notably different from conventional phase or amplitude gratings. Although its natural eigenpolarizations are circular (i.e., the Stokes V parameter), the PG beamsplitter

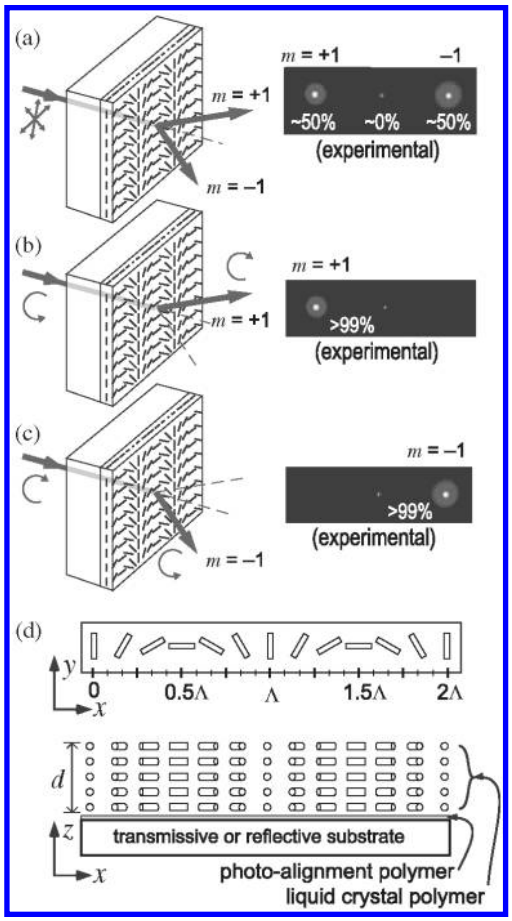

FIG. 1.—Basic PG behavior: (*a*) incident linear or unpolarized light splits equally into the two first orders; incident (*b*) left and (*c*) right circularly polarized light diffracts fully into only one of the first orders, and (*d*) top and side views of the nematic director field structure of the narrowband PG. The periodic pattern of lines indicates the local orientation of the extraordinary axis (n_e) of the birefringent LCP. As a more detailed view, the cylinders in (*d*) represent the spatial nematic director orientation, where the long axis also corresponds to n_e. Illustrations adapted from McManamon et al. (2009) and Escuti & Jones (2006). See the electronic edition of the PASP for a color version of this figure.

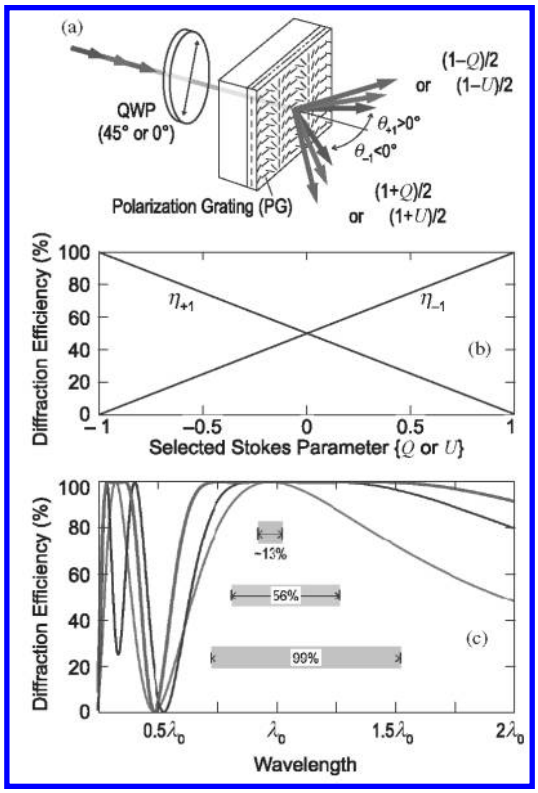

FIG. 2.—Polarization behavior and broadband PGs: (*a*) arrangement of PG with a QWP sensitizing the diffracted intensities to linearly polarized light (i.e., Q and U), (*b*) calculated peak first-order diffraction efficiencies $\eta_{\pm 1}$ as a function of input polarization (note $\eta_0 = 0$ throughout), and (*c*) spectra of total first-order efficiency ($\eta_{+1} + \eta_{-1}$) for three types of PGs—narrowband (eq. [1]), broadband type I (Oh & Escuti 2008), broadband type II (eq. [2]). Note that when $\lambda_0 = 20$ μm, then the range of plot (*c*) is directly comparable with the wavelength range in Figs. 3, and 7–9. See the electronic edition of the PASP for a color version of this figure.

can be paired with a quarter-wave plate (QWP) in order to separate incident light based on any eigenpolarization desired (e.g., Q, U) (Escuti et al. 2006), as illustrated in Figure 2a. The result is that the diffraction efficiency of the $m = +1$ and $m = -1$ orders are linearly proportional to the selected Stokes parameter, as plotted in Figure 2b. Furthermore, the precise 3D nematic liquid crystal (LC) director structure determines the spectral behavior. The simplest LC structure found in conventional PGs, illustrated in Figure 1d, leads to what is called a narrowband PG, in which first-order diffraction efficiency follows (Escuti et al.2006; Oh & Escuti 2007b; Nikolova et al.1984):

$$\eta_{\pm 1} = \left(\frac{1 \mp V}{2}\right) \sin^2 \Gamma, \qquad (1)$$

where V is the incident light's normalized Stokes vector component corresponding to its fraction of elliptical polarization, $\Gamma = \pi \Delta n d/\lambda$, $d = \lambda_0/(2\Delta n)$ is the film thickness, λ is the wavelength, and λ_0 is a fixed wavelength parameter near the center of the bandwidth. Note that the $m = 0$ (zeroth-order) efficiency is always $\eta_0 = 1 - \eta_{+1} - \eta_{-1}$. This narrowband PG is known to have greater than 99% efficiency at optical wavelengths in both theory and experiment (Escuti et al. 2006; Kim et al. 2008), but only at wavelengths close (within $\Delta\lambda/\lambda_0 \sim 13\%$) to the half-wave retardation condition ($\lambda_0 \sim 2\Delta n d$). However, as can be observed from Figure 2c, this is a small fraction of the wavelength range of interest in this article (5–40 μm).

However, two additional broadband PGs with modified nematic director profiles have been identified, with high-efficiency bandwidths ($\Delta\lambda/\lambda_0$) increased by up to eightfold. A two-layer broadband PG (Oh & Escuti 2008), which we will call "type I" here, offers a bandwidth of ~56% (shown in Fig. 2c). And the most broadband PG yet identified (Escuti & Oh 2007) is composed of three layers, which we will call "type II" here, and has efficiency that follows:

$$\eta_{\pm 1} = \left(\frac{1 \mp V}{2}\right)(1 - (\cos^3 \Gamma - \cos \Gamma \sin^2 \Gamma(1 + 2\cos(2\Phi)))^2), \quad (2)$$

where $\Phi = 53°$, and all other parameters are defined the same equation (1). In this case, the total thickness of the film is $3d \sim 3\lambda_0/(2\Delta n)$. As can be seen in Figure 2c, this broadband PG (type II) has a bandwidth of $\sim 99\%$ and is therefore the PG we will employ in the section on design and discussion (§ 5). However, we will use narrowband PGs (eq. [1]) in § 4, since fabrication is easier and interpretation of measurement results is more straightforward.

As the component is a grating, the resulting beams are spectrally dispersed, as well as being sorted into a polarization state, as shown in Figure 1e, following the grating equation:

$$\sin \theta_m = m\lambda/\Lambda + \sin \theta_{\text{in}}, \quad (3)$$

where Λ is the grating period, θ_m is the diffraction angle of order m, and θ_{in} is the incidence angle. Alternatively, the groove frequency $\text{GF} = 1/\Lambda$ of the grating may be employed rather than the period. At optical and near-infrared wavelengths, PG diffraction efficiency has been shown to be greater than 99% (nearly no absorption or scattering), diffracting incident light into one of only three orders ($m = 0, \pm 1$) based on the incident polarization state (see Figs. 1a–1c).

In NCSU's nearly ideal experimental gratings, the $m = 0$ beam is unpolarized, but contains typically less than 0.5% of the incident flux when optimized for visible wavelengths (Escuti & Jones 2006) and less than 0.125% when optimized at 1.55 μm (Kim et al. 2008). The $m = \pm 1$ orders are orthogonally polarized with extinction ratios greater than 1000 s:1 (Oh & Escuti 2008), making the PG component a very attractive potential alternative to other analyzers. A PG has an extinction ratio of greater than 10^3, whereas a wire grid polarizer is typically greater than 10^2, and a Wollaston prism has an extinction ratio greater than 10^6. The effect of a lower extinction ratio is a less efficient polarimeter, but this effect can be well quantified and corrected for, as the effect is typically unchanging. Several wire-grid-based polarimeters were in regular use before Wollaston-prism-based polarimeters, so the extinction ratio of PGs is not expected to be a major problem. Note that although Figure 1 shows the transmissive configuration, the reflective mode is completely analogous (Komanduri et al. 2009).

Polarization gratings are currently being developed at NCSU as polymer films and electrically switchable diffractive elements for ultraefficient liquid crystal displays, nonmechanical optical beam steering, and telecommunication devices, variously funded by the NSF and the US Air Force Research Laboratory, among others. Although this article focuses on PGs formed with LCP materials, since they offer relatively convenient processing for visible/NIR wavelength operation, it is important to note that the periodic birefringence pattern necessary for PG behavior can also be formed by other means and materials. In particular, form birefringence can result from subwavelength gratings (Bomzon et al. 2001; Hasman et al. 2002) formed in bulk solids (e.g., intrinsic Si). Therefore, the primary aspect of this work is to examine the suitability of LCP-based PGs for MIR operation, but a secondary aspect is to also discuss the MIR potential of PGs (formed by any means and materials).

3. MEASUREMENT TECHNIQUES

3.1. Introduction

To investigate the applicability of PGs for a MIR polarimeter, we produced several test-samples of unpatterned (i.e., wave plates) and patterned (i.e., PGs) LCP films in the NCSU laboratory. Although a detailed fabrication description of each is provided in §§ 4.1 and 4.2, respectively, note that all films were deposited on a silicon slide, and all measurements were performed only in transmission mode. The LC film thicknesses were optimized to MIR wavelengths based on extrapolations of the NIR response of a similar PG, but no iterations between measurements and production were made, due to time and cost constraints. The measurements of the sample pieces were made at the College of Optics and Photonics, Center for Research and Education in Optics and Lasers laboratory, at the University of Central Florida.

3.2. MIR Ellipsometry

A Woollam IR-VASE (variable-angle spectroscopic ellipsometer) was used in the characterization of the optical properties of the thin-film LCP used in the development of the PG. The IR-VASE has a typical operating spectral range of approximately 2–30 μm, with the spectral range determined by the IR-VASE's source (a glow bar) and the cutoff of the optics in the system. A standard measurement process for the ellipsometer is described in detail in Woollam et al. (1999). We note that the ellipsometer, when not in FTIR (Fourier transform infrared spectroscopy) mode, measures the field amplitude ratio (Ψ) and phase shift (Δ) of the surface under test. These terms are related to the measured change in polarization upon reflection from the test surface by

$$\rho = \tan(\Psi)e^{j\Delta} = R_P/R_S, \quad (4)$$

where R_P is the ratio of the reflected and incident *parallel* polarized light and R_S is the ratio of the reflected and incident *senkrecht* polarized light. The measured Ψ and Δ can then be fit using an oscillator model using software provided by the manufacturer for determination of the optical properties of the surface.

Complete characterization of the LCP film requires additional steps beyond the characterization a typical isotropic thin film. Initial measurements were carried out to determine the optical properties of the substrate and the LCP's alignment layer

using standard isotropic analysis. Once these values were known, the complete LCP stack-up was measured in multiple configurations over several angles: anisotropic reflection scan with the LCP on a ground plane, anisotropic reflection scan with the LCP on a transparent substrate, and anisotropic transmission scan with the LCP on a transparent substrate. From the results, the two measurements on the transmissive surface were selected for further analysis. Two Kramers-Kronig (Fox 2001) consistent models were developed to predict the optical properties of the ordinary and extraordinary axes of the birefringent LCP. These two models were combined into a single anisotropic model and fit to the measured results over the largest band possible to ensure the most accurate results.

3.3. FTIR Absorption Measurement

Measurement of the absorption properties of the LCP films was performed using a standard FTIR and the IR-VASE spectroscopic ellipsometer. The FTIR employed was a Perkin-Elmer micro-FTIR spectrometer with a spectral range of 2–22 μm. The spectrometer includes a microscope attachment that allowed for minimization of the surface area tested. This reduced the error introduced due to film nonidealities such as film stress. Later measurements were carried out using the FTIR option on the IR-VASE, to extend the measured spectral range to 25 μm. However, the IR-VASE measured a larger area of the substrate ($\geq$5 mm diameter), as compared with the standard FTIR (less than 2 mm diameter). As the initial samples showed a high degree of uniformity in regions $\sim$2 mm^2, the larger beam size of the IR-VASE degraded the overall accuracy of the optimal sample performance. For normalization, additional measurements were carried out using the substrate only.

3.4 MIR Diffraction Measurement

We illuminated PG samples with a polarized collimated CO2 laser beam ($l = 10.6$ μm), normally incident, and measured the transmitted power in both the (diffracted) off-axis and (directly transmitted) on-axis directions. The laser was a water-cooled LASY-5S, produced by Access Laser Company, operated in TEM (0,0), with $M^2 < 1.1$. The beam width was 2.4 mm in diameter, with a 5.5 mrad divergence. The beam was linearly polarized horizontal, parallel to the base of the laser. Ideally, all of the input power would be directed in either of the two ($m \pm 1$) diffraction paths ($\pm 4.65°$ off-axis). For these diffraction measurements, we distinguish between two quantities: transmittance T and diffraction efficiency η. The transmittance (defined in this case as the net throughput) is the ratio of the power contained within a diffraction order m to the incident power $T_m = P_m/P_{\text{in}}$ and containing all losses in both the grating and substrate, including absorption, scattering, reflection, and diffraction leakage. The diffraction efficiency is defined as the ratio of power within a diffraction order m to the total power within all diffraction orders $\eta_m = P_m/(\cdots P_{+1} + P_0 + P_{-1} \cdots)$ and contains only the effect of the diffractive ability of the grating (i.e., no absorption, scattering, refection, or substrate effects).

3.5. Polymer Film Thickness Measurement

We measured LCP film thickness with a stylus profilometer (Tencor Alpha Step). Several macroscale scratches were formed at several locations on each sample with a razor blade, and the step height of each was measured.

4. RESULTS/DISCUSSION

In this section, we report the behavior of PG, formed with LCP materials at MIR wavelengths (2–38 μm). Three primary questions drive this initial work: (1) Do PGs operate as diffractive polarizing beamsplitters over this wavelength range? (2) What is the throughput over this wavelength range? (3) What are the principal opportunities for improvement? With answers to these questions, we can estimate the overall throughput of PGs at 5–40 μm, as required based on the science drivers for a SOFIA-based polarimeter. We first measure LCP material properties using wave plate samples (§ 4.1) and subsequently use this information to design, fabricate, and measure the narrowband polarization and diffractive behavior of patterned PG samples (§§ 4.2 and 4.3).

4.1. Measured Birefringence and Absorption

For our candidate material, we selected the LCP RMS03-001C (Merck Chemicals), since it is commercially available and often used for polarization gratings (Oh & Escuti 2008; Escuti et al. 2006) at visible wavelengths. Conventionally, this LCP is used to form wave plates and retardation compensation films for LC displays, and it is important to note that many LCP materials exist (Kelly 1995) based on a wide variety of chemistries. When fully uniformly aligned and polymerized using standard solvent coating techniques, this LCP film has uniaxial optical symmetry and at 589 nm has a nominal birefringence $(\Delta n) \sim 0.15$ and negligible absorption at optical wavelengths.

In order to measure the basic LCP material parameters, we began by preparing LCP wave plates. We prepared a uniformly aligned layer of LCP with thickness of 9.4 μm $\pm$ 0.2 μm on an undoped Si wafer, such that the extraordinary axis was in plane (Fig. 3a). The wafer was a standard commercial-grade high-resistivity 3 inch float-zone silicon wafer, 380 um thick, polished on both sides. First, we spin-coated an alignment material (a 50 nm thick photoalignment polymer [Schadt et al. 1996]) on the Si substrate and allowed it to dry. Second, we exposed this alignment layer with a spatially uniform, linearly polarized, UV (325 nm) illumination, capturing the uniform linear pattern onto the surface. Third, we applied a solution containing LCP material by spin-coating, allowing it to dry and allowing the LC to align according to the surface pattern. Finally, we polymerized the LCP film by a second blanket, unstructured, UV

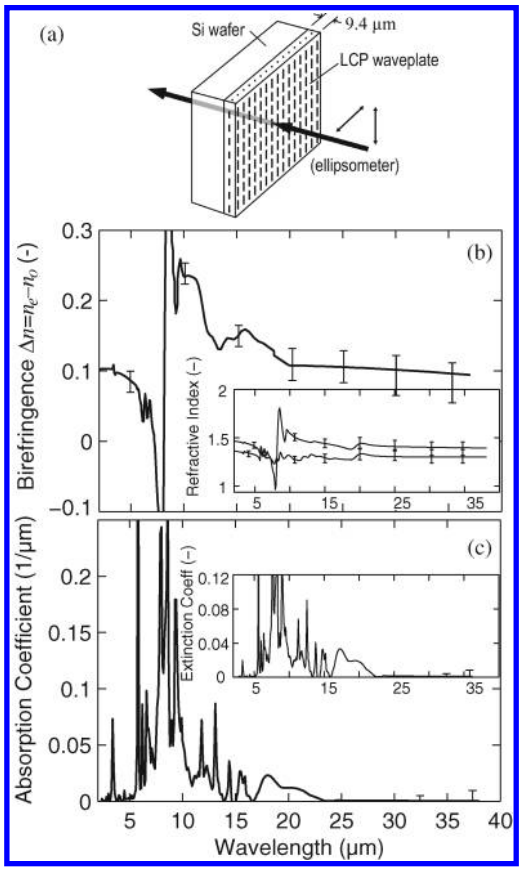

FIG. 3.—Measured LCP birefringence and absorption: (a) illustration of the LCP wave plate tested; (b) birefringence spectrum (inset: refractive index); and (c) absorption coefficienct spectrum (inset: extinction coefficient).

exposure, in order to harden the film and fix the LC alignment permanently. The final LCP thickness was achieved by repeating these spin-coating and polymerization processes.

Using the ellipsometry techniques described previously, the extraordinary refractive index n_e, ordinary refractive index n_o, and extinction coefficient k were measured throughout the 2–38 μm wavelength range. From this data, the birefringence $\Delta n = n_e - n_o$ (shown in Fig. 3b) and the absorption coefficient $\alpha = 4\pi k/\lambda$ were calculated. The latter was also measured using an unpolarized FTIR, which corresponded well with the ellipsometry data, but at a finer wavelength resolution. In Figure 3c, we show the absorption coefficient, where the range of 2–25 μm only shows the FTIR data, for clarity. Note that the refractive index and extinction coefficient data are shown as insets to Figures 3b and 3c, respectively.

These parameters have direct impact on the detailed PG behavior. Most importantly, note that a substantial birefringence ($\geq$0.1) persists throughout most of the wavelength range, except near the major absorption resonances between ~6 and 10 μm. Note that while the exact atomic composition of this LCP is confidential to the vendor (Merck), these molecular vibration absorption modes in LCP in general are primarily related to the HC_x, C = C, C-C, C = O, C-O, and C-N bonds. Furthermore, note that the absorption is modest at wavelengths greater than 10 μm, which suggests that PGs made from this material should have low absorption loss compared with alternative beamsplitter technologies, which is a central argument to consider PGs over conventional crystalline Wollaston prisms, such as those constructed from the CdSe or CdS.

As will be more fully described in the following sections, we measured the LCP birefringence and the net absorption coefficient at MIR wavelengths using three largely independent techniques, using both uniformly aligned and grating samples. Table 1 summarizes these results for the 10.6 μm CO_2 laser wavelength and shows that they all appear consistent.

4.2. Measured Polarization Behavior

Until now, we have exclusively examined the material properties of the LCP. In this section, we examine the polarization, diffraction, and throughput behavior of a sample PG formed with that LCP. Several photographs of an example PG are shown in Figures 4a and 4b. A series of narrowband PGs were formed with a 131 μm grating period ($\pm$4.65° first-order diffraction angle for 10.6 μm wavelength) on undoped Si substrates (Fig. 4d). These were prepared in a manner similar to the preceding samples, with the exception that the alignment layer was exposed using polarization holographic lithography (Nikolova & Todorov, 1984; Crawford et al. 2005). Two orthogonal, circularly polarized, coherent, UV beams from a HeCd laser (325 nm) were superimposed to create a periodic interference pattern with constant intensity and spatially varying linear polarization orientation. This light profile creates the periodic surface condition that after spin-coating the LCP leads to the PG structure illustrated in Figure 1d. We adjusted the LCP thickness (between 23 and 34 μm) by controlling the spin speed and solvent-to-solids concentration of the LCP mixture.

TABLE 1
MEASUREMENT SUMMARY OF BIREFRINGENCE AND ABSORPTION COEFFICIENT FROM MULTIPLE MEASUREMENT TECHNIQUES AT $\lambda = 10.6$ μm.

Parameter	Ellipsometry	FTIR	Laser diffraction
Birefringence $\Delta n = n_e - n_o$	0.235 ± 0.02	...	0.20 ± 0.015
Net absorption coeff α (μm^{-1})	0.032 ± 0.008	0.028 ± 0.004	0.032 ± 0.002

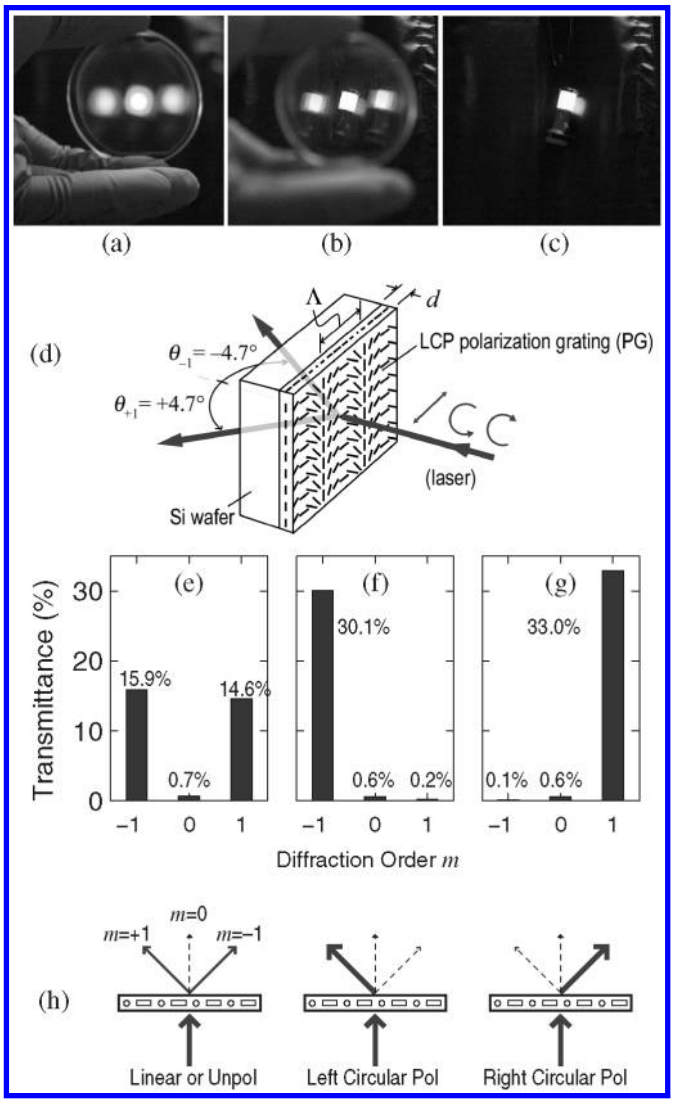

FIG. 4.—Measured diffraction of MIR narrowband PGs formed with LCP at 10.6 μm laser wavelength: (*a*) photograph of transmissive PG showing the first- and zero-order diffraction images of a lamp arranged behind it, (*b*) similar to (*a*), but the camera is focused on the lamp and images are better resolved, (*c*) photograph of lamp alone, without PG, (*d*) illustration of the PG tested; (*e*)–(*g*) measured transmittance in each diffraction order for various input polarizations, and (*h*) polarizations and illustrations of the measurement of (*e*)–(*g*). See the electronic edition of the PASP for a color version of this figure.

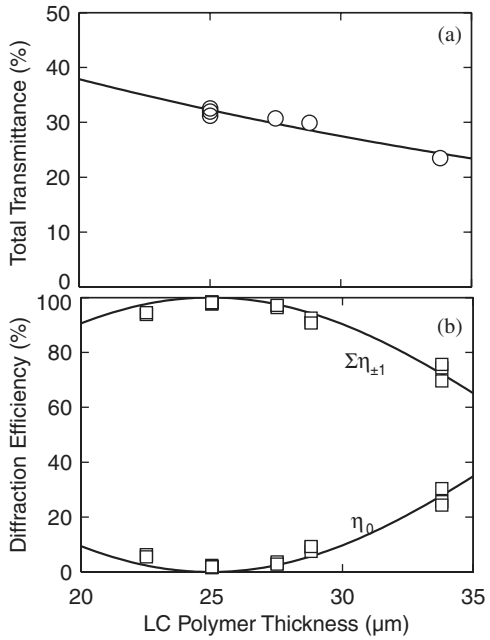

FIG. 5.—Measured MIR narrowband PG throughput at 10.6 μm laser wavelength: (*a*) total transmittance into any forward direction and (*b*) diffraction efficiency of first and zero orders. Note that discrete points are measured data, while curves are theoretical fits employing eqs. (1) and (5).

We first consider the transmission of the PG. Figures 4 and 5 show that the total loss of flux was approximately 70%, depending on LCP thickness. Note that this loss has two primary components. First, throughput loss of the raw Si reference substrate was ~30%, due primarily to the Fresnel reflection at the Si-air and LCP-air interfaces; note that no antireflection coatings were employed that would have significantly reduced the interface losses and that several low-temperature deposition techniques for this are available for use on polymer films. Second, as we were unable to observe any scattering at visible or MIR wavelengths in the films, virtually all of the remaining throughput loss is due to absorption within the PG (i.e., 55–68% absorbance of the LCP alone, depending on thickness), and from this we can estimate the absorption coefficient of the PG (included in Table 1). Note that while this absorption coefficient is substantially higher than that of a Wollaston prism, the optical path length is dramatically smaller. An expanded discussion on the comparable performance is included in § 5.1.

Polarized transmittance measurements confirmed that the PGs behaved as an excellent polarizing beamsplitter at 10.6 μm, similar to all prior characterizations at visible/NIR wavelengths. In 4, we report the transmittance (i.e., net throughput) into the main diffraction directions for a PG with a 25 μm LCP thickness, for three input polarizations (linear, left-handed circular, and right-handed circular). The eigenpolarizations of this polarizing beamsplitter are manifestly circular, as Figures 4f and 4g show, with a strong polarization extinction ratio as high as 375:1.

4.3. Measured Diffraction Behavior

We prepared a series of PGs with a range of LCP thicknesses and with otherwise identical parameters. In Figure 5a, we report the total transmittance (in all orders) at various thicknesses. We then found the least-squares-error fit with equation (1) combined with equation (5) to determine the absorption coefficient at this wavelength as $\alpha = 0.032\ \mu\text{m}^{-1}$, very similar to the value measured by ellipsometry and FTIR. We confirmed that the

power measured at higher diffraction orders ($m \geq |2|$) was negligible ($\eta < 0.2\%$).

We also calculated the zero- and total first-order efficiency, which enables us to observe the behavior of the grating as a spectroscopic dispersing element, where the effects of the substrate, interface reflections, and all absorption were normalized and then removed. The measured diffraction efficiency is shown in Figure 5b, where it is notable that the maximum measured total first-order diffraction efficiency was 98.2% ($\pm 1\%$); this confirms that apart from absorption and Fresnel reflections at interfaces, the PG itself is a nearly 100%-efficient diffraction grating (the same quality as at visible/NIR wavelengths). We then found the least-squares-error fit (with narrowband efficiency defined in Oh & Escuti (2007b) and Escuti et al. (2006) to determine the birefringence at this wavelength as $\Delta n = 0.20$, very similar to the value measured by ellipsometry.

With these diffraction and polarization measurements, we confirm the essential and unique behavior of PGs formed with LCP materials operating at MIR wavelengths: high diffraction efficiency into the first orders, strong polarization dependence, low scattering, and modest anticipated overall transmission loss.

5. APPLICATION OF PG FOR MIR ASTRONOMY

In this section, we discuss the principles of designing PGs for the wide MIR wavelength range of interest to SOFIA. We also apply the data measured in § 4 of our candidate LCP and predict the throughput in this case. Finally, we speculate on the potential best-case performance when using an optimized LCP material of the same family.

5.1. Design of Broadband PGs as Polarizing Beamsplitters for MIR Polarimetry

The bandwidth of 5–40 μm for a SOFIA-based polarimeter is extremely large ($\Delta\lambda/\lambda_0 = 156\%$), and as a result, more than one PG is necessary to cover this range. In addition, more than one type of detector array is needed, as discussed in Packham et al. (2008), and both of these constraints guide the optical and system design. In this section, we identify an optimum design for the number and properties of PGs optimized to enable the highest efficiency possible throughout the entire wavelength range.

In the context of a polarimeter, the PG functions to a first approximation as a diffractive, polarizing beamsplitter, where the $+1$ and -1 diffraction orders comprise the two orthogonally polarized output beams. Therefore, the total beam separation Θ of the two orthogonal polarization modes will inherently depend on the wavelength, grating period (or groove frequency, GF), and incident angle, described in equation (3) as follows: $\Theta = \theta_{+1} - \theta_{-1} = 2\theta_{+1}$, at normal incidence. The angular dispersion also follows classic diffraction grating behavior, so it is therefore coupled with the beam separation angle. The beam separation angle is shown in Figures 6a–6c, for several choices

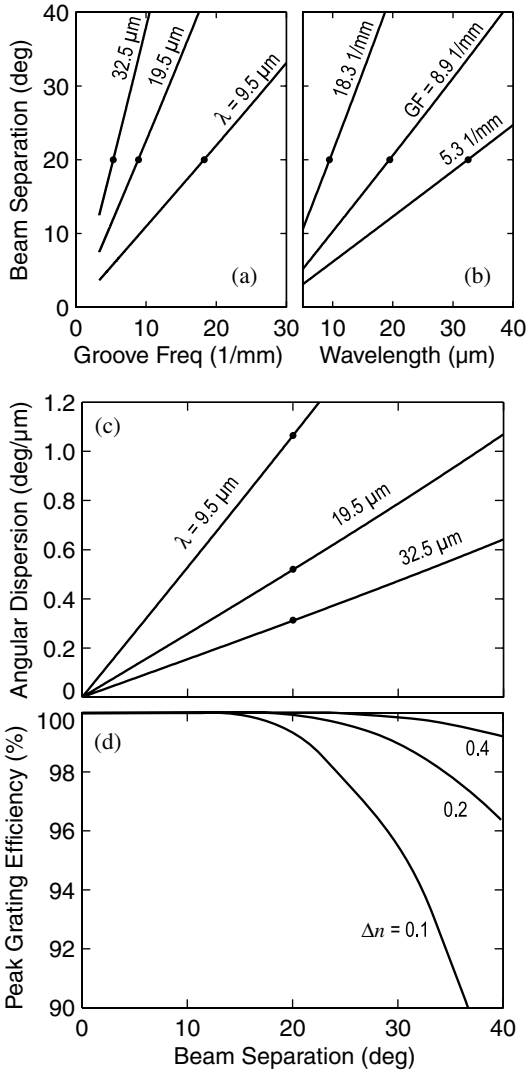

FIG. 6.—PG diffractive beam splitting characteristics: (*a*)–(*b*) beam separation between the $+1$ and -1 diffraction orders, for several λ and GFs, (*c*) angular dispersion, as governed by the grating equation, and (*d*) peak first-order efficiency for several values of birefringence Δn, as calculated using finite difference time-domain numerical simulation (Oh & Escuti 2006). Note that the discrete points correspond to the design points in Table 2 and surrounding discussion.

of λ and GF. It is important to note that substantial values of Θ are feasible. For discussion purposes, we will choose a $\Theta = 20°$, indicated within Figure 6, which, along with the next discussion, directly leads to most of the parameters in Table 2.

While the efficiency in equation (3) (and eq. [1]) is exactly valid for small diffraction angles, the PG manifests more zero-order leakage and lower first-order efficiency than the expression predicts as the diffraction angle increases. The physical principals leading to this effect are discussed in Oh & Escuti (2008) for the narrowband PGs and are similar for the broadband variants. These effects so far can only be accurately modeled using numerical simulation tools, such as the

TABLE 2

DESIGN PARAMETERS FOR THREE BROADBAND (TYPE II) PGS TO COVER 5–40 MM WAVELENGTH RANGE.

Design Parameter	PG 1	PG 2	PG 3
Wavelength range (μm)	5–14	14–25	25–40
Center wavelength (μm)	9.5	19.5	32.5
Beam separation, center wavelength (deg)	20	20	20
Groove frequency (1/mm)	18.3	8.9	5.3
Grating period (μm)	54.7	112	187
LCP half-wave thickness d (μm)	30	63	120

finite-difference time-domain method adapted to birefringent media (Oh & Escuti 2006), since it is important to include both the vector nature of light and the inhomogeneous anisotropic media, as well as the wave response to features with size commensurate to the wavelength. We summarize the efficiency roll-off in Figure 6d for various birefringence values. The two most important points are that higher Δn leads to higher efficiency at higher angles and that even a value of $\Delta n = 0.1$ allows for high efficiency out to $\Theta = 20°$.

The most suitable focal-plane arrays are based on Si:As and Si:Sb detector materials (Adams et al.2006; Packham et al. 2008), where the MIR bandwidth of interest is divided into 5–25 μm and 25–40 μm windows, respectively. Furthermore, the shorter window must be subdivided further into 5–14 μm and 14–25 μm, in order to allow this broadband PG (with bandwidth $\Delta\lambda/\lambda_0 < 90\%$) to manifest high efficiency throughout, as detailed in Table 2.

By combining the measured birefringence data (Fig. 3b) with equation (2), we can now estimate the diffraction efficiency across the entire MIR range of interest for the LCP under test and choose the optimal thicknesses for each PG. The result of this optimization is shown in Figure 7, leading to the set of design parameters listed in Table 2. This design leads to very high diffraction efficiency across nearly the entire 5–40 μm range, with the exception of 6–10 μm, where the birefringence of this LCP varies significantly from the nominal 0.1–0.2 range.

The total throughput T_{tot} of the two orthogonally polarized beams of a physical PG thin film is composed of several elements and may be estimated in reflective and transmissive modes by the following:

$$T_{\text{tot}} = \eta_{\pm}\eta_{\text{abs}}\eta_{\text{refl}}, \tag{5}$$

where $\eta_{\pm 1}$ is the first-order diffraction efficiency of the grating itself (defined here by eq. [2]). The quantity $\eta_{\text{abs}} = \exp(-\alpha d')$ is the fraction of light not absorbed through an LCP film (where $d' = 3d$ for the broadband PG discussed previously). For the transmissive configuration, the quantity $\eta_{\text{refl}} = (1-R)^2$ is the fraction of light not reflected at the two polymer-air interfaces, where the reflectance of each interface determined by the Fresnel equation: $R = ((n-1)^2 + k^2)/((n+1)^2 + k^2)$. For the reflective configuration, $\eta_{\text{refl}} = (1-R)$ for the single polymer-air interface. For simplicity, we have here neglect the influence of the substrate, which in reflective PGs is likely to be only a refinement on the estimate in equation (5).

We now estimate the throughput of broadband PGs on a gold mirror substrate using the current LCP material (a configuration illustrated in Fig. 8a). By combining the measured properties (Fig. 3) and efficiency estimate (Fig. 7) into equation (4), we calculate the total PG throughput T_{tot}, as shown in Figure 8b.

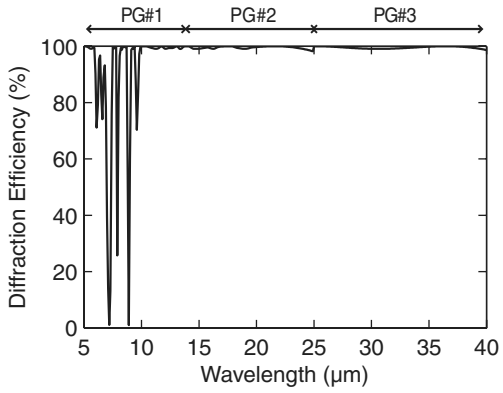

FIG. 7.—PG diffraction efficiency, calculated for three PGs to cover the three wavelength bands, as described in Table 2, using measured birefringence and theoretical efficiency equations. Note that grating efficiency only includes the effects of diffraction and does not include the effects related to absorption or substrates.

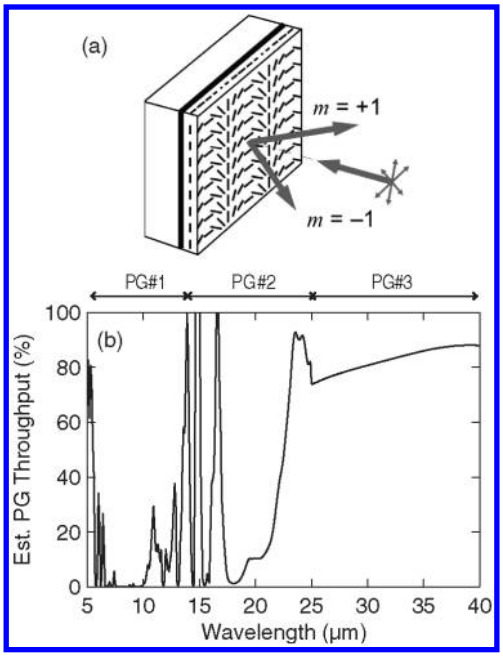

FIG. 8.—Throughput of a three-PG-based system, using the candidate LCP material characterized here: (*a*) illustration reflective mode PG and (*b*) estimated net throughput (assumptions described in text), where loss throughout is principally due to LCP absorption. See the electronic edition of the PASP for a color version of this figure.

For this calculation, we have assumed a perfect antireflection coating to eliminate the Fresnel-type reflection losses at the interfaces. Further, the throughput is for a single PG, but in the case of a linear polarimeter, conversion to circularly polarized light is necessary, which can be accomplished through use of an additional element acting as a QWP. The expected throughput of a QWP formed with LCP materials will be similar in envelope to that shown in Figure 8b, albeit with increased throughput at all wavelengths, because it will be thinner, but it could be substantially higher if a non-LCP material is used.

The MIR instrument CanariCam has polarimetric optics (using a crystalline polarimetric optics) and a diffraction grating optimized for operation between 7.5 and 13.5 μm. If these optical elements are introduced into the beam simultaneously, the same net effect as with the PG is achieved. The total throughput of both the polarimetry optics and grating reaches as high as $\sim 80\%$, falling to $\sim 35\%$ by 20 μm, but at wavelengths longer than ~ 23 μm it is nontransmissive. In our test case, the PG sample throughput compares very similarly with that of the peak throughput of CanariCam for all wavelengths greater than 25 μm, but it is inferior at wavelengths between 7 and 25 μm. However, we note that the cost for the CanariCam polarimetry optics was tens of thousands of dollars, it was the largest available prism that could be produced at that time, and the delivery time was many months. A PG can be produced in a very large format (currently produced up to 150 mm diameter in NCSU's academic research setting and expected to be produced in sizes up to 300 mm), can be produced within a few weeks, and is relatively inexpensive to produce (a few hundred dollars). Furthermore, the PG throughput can likely be improved (see § 5.2) with a view toward expanding the low-loss bandwidth.

5.2. Prediction of Enhanced Reflectance

While the current LCP material has proven to be feasibile for PGs in MIR polarimeters, it is clear that solutions with less absorption are necessary. Many optimization techniques are known in the liquid crystal community that can increase the birefringence (while perhaps decreasing absorption), via modified chemical structures and guest-host doping. For example, the family of iosothiocyanato-tolane LCs (Gauza et al.2003) with birefringence in the range of 0.4–0.6 (currently, only characterized at near-IR wavelengths and below) offers a four- to- sixfold improvement in the birefringence from similar materials. An additional avenue we plan to examine is doping with single-walled carbon nanotubes (Fagan et al.2007), which offers very low absorption and very high birefringence at 5–40 μm. Our current best estimate is that these developments could lead to birefringence values of around $\Delta n \sim 0.8$ at MIR wavelengths, *enabling much thinner PGs* and hence *significantly less absorption*. Assuming this factor-8-higher birefringence, and otherwise using the measured data in Figure 3, we estimate a revised total throughput in Figure 9, where the throughput gain arises because all LCP layers are projected to be factor-8-times thinner.

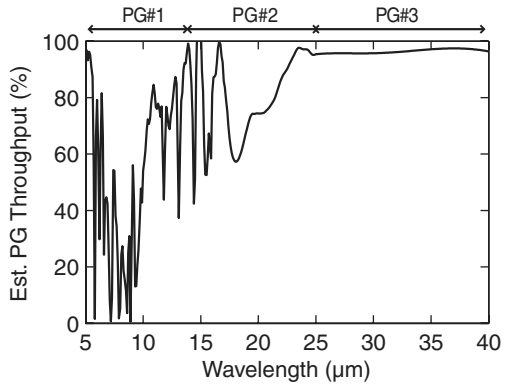

FIG. 9.—Predicted throughput of a PG-based system, using an optimized LCP with higher (factor of 8) birefringence LCP material, but the same absorption coefficient. Reflective mode is assumed, as in Fig. 8.

The net result is a substantially higher throughput, especially at wavelengths greater than 10 μm, representing a realistic potential performance with a modest amount of additional development. Note also that low-loss narrowband form-birefringence PGs for MIR wavelengths have been studied (Bomzon et al. 2001; Hasman et al. 2002), and there is a strong possibility that they could be enhanced by structuring the out-of-plane dimension to achieve a broadband PG with very little absorption anywhere in the wavelength range of interest. If this avenue is successful, then a PG could be formed in a solid-state material (e.g., intrinsic Si), which would have birefringence governed by the subwavelength surface structure and absorption governed by the bulk material. Overall, this best-of-both-worlds scenario may offer the lowest absorption and widest bandwidth for PGs at MIR wavelengths, but requiring more developmental efforts.

5.3. PG Survivability and Behavior at Cryogenic Temperature

It is important to note that both the initial fabrication and all measurements of the LCP were made at room temperature. Nevertheless, the optical and mechanical behaviors of PGs at the operational cryogenic temperatures are undoubtedly critical for polarimetry across the MIR range, as the PGs will be situated within a cold ($\sim$20 K) dewar. As an initial study of these effects, we placed several uniformly aligned LCP films within a cooling stage (Linkam) and measured the birefringence (Escuti et al. 2004) at optical wavelengths down to liquid nitrogen temperature (76 K). Figure 10 shows the result, where the birefringence varies little (less than 3%) to 76 K. As the majority of the mechanical contraction of the substrate occurs between room temperature and 76 K, we expect very little additional change when cooling to less than 76 K. After cycling to the low temperature and back to room temperature several times, the films remained intact and well-adhered to the substrate—as expected, since the LC material composing the PG is a highly cross-linked polyacrylate network (Broer et al.1989).

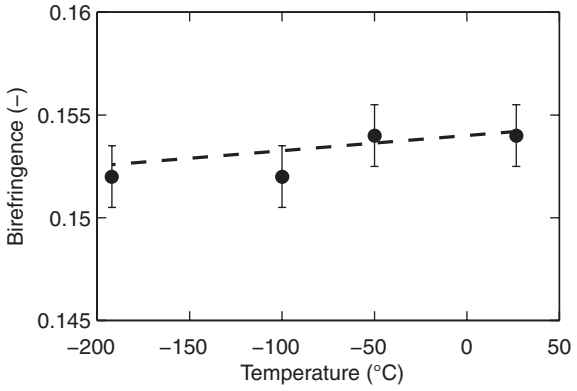

FIG. 10.—Measured birefringence of candidate LCP, at 633 nm wavelength and scan rate of approximately $-2°\text{minute}^{-1}$.

5.4. PG Throughput, Optical Quality, Size, and Cost

Through experimentation with doping of the LCP material that constitutes the PG, it is hoped that the high level of throughput seen at ≥ 25 μm can be extended to wavelengths as short as 1 μm. Improved doping of the LCP may also provide a birefringence at the same or higher level at wavelengths as short as 1 μm. PGs are routinely produced to a diameter of 50 mm, and test pieces have been produced up to 150 mm diameter. Future funded projects aim to increase the diameter to 300 mm, where the size limit is the holographic exposure optics and laser power needed for the alignment layer. The CanariCam CdSe Wollaston prism is (to the authors' knowledge) the largest MIR Wollaston yet produced and close to the maximum size possible to produce, with a size of 33×38 mm. Crystalline Wollaston prisms optimized for other wavelengths (e.g., optical, near-IR) have similar size limitations. PGs are already ~ 4 times larger than the CanariCam Wollaston prism and are expected to reach almost an order-of-magnitude larger size within the coming years. The costs for a PG in comparison with a Wollaston prism are significantly lower; current production costs for a PG are a few hundred dollars, in comparison with several tens of thousands for large Wollaston prisms. The time required for production of a PG is a few days, in comparison with that of several months for a large crystalline Wollaston prism.

Although we did not measure our MIR gratings for wavefront error, prior tests of NIR PGs deposited on glass substrates (unpublished) shows the wavefront quality to be ~ 0.25 peak-to-valley waves and 0.05 rms waves across an area of approximately 10×10 mm^2 at 633 nm. We concluded that this was approximately the quality of the substrates used, and therefore the PG contributed negligibly to the wavefront error. Future work on PGs at MIR wavelengths must test this at the wavelength of operation.

Despite the advantages of PGs, a Wollaston-prism-based polarimeter maintains some advantages. Chief among these is that intrinsic to the PG, the incident light is dispersed in both the polarimetric and spectroscopic domains, making the design of an imaging polarimeter difficult with a PG. The currently measured peak throughput of 80% is similar to that obtained in the CanariCam spectropolarimetry mode, but at a wavelength ≥ 25 μm, which, although ideal for a SOFIA-based polarimeter, is not currently competitive at shorter wavelengths. We note that PGs optimized for optical and 1–5 μm are available, but further work on doping the LCP is needed to obtain the wide bandwidth needed for a SOFIA-based polarimeter. Repetitive cold-temperature cycling must be demonstrated, but the initial tests indicate little or no degradation. Finally, attention to the uniformity of the surface structure is needed to extend it to larger PGs with the required high degree of optical quality.

6. CONCLUSIONS

We have characterized narrowband PGs at MIR wavelengths, formed with a commercial candidate LCP material, and discussed the design of broadband PGs. Through measurements of the birefringence, throughput, spectral dispersion, and temperature cycling, we have demonstrated that the current-generation PGs are excellent candidates for a SOFIA-based polarimeter at wavelengths ≥ 25 μm, and future work will investigate extending high and stable birefringence and throughput to shorter wavelengths. Careful characterization of a PG-based polarimeter can account for the slightly lower polarimetric efficiency when compared with a Wollaston-prism-based system.

Much work remains with the optimization of the PGs at MIR wavelengths, and we note again that optical and near-IR PGs are already in common use in applications such as liquid crystal displays, nonmechanical optical beam steering, and telecommunication. PGs could be well used in astronomy, where the often-competing requirements of a large cold pupil (due to large telescopes and/or to maximize the spectral resolution) contrasts with the size limits of the analyzer, leading to a compact pupil size requirement for polarimetry. Further, a LCP-formed QWP can be used to modulate the polarization of the incident beam instead of a crystalline wave plate. The location of the modulation should occur as far upstream in the optical path of the instrument as possible, often leading to a large beam size, for which it can be difficult to produce a sufficiently large retarder. PGs are poised to offer an order-of-magnitude increase in size over crystalline components, at a fraction of the cost. We plan to continue our characterizations of PGs to continue our design ready for SOFIA's next call for instruments. We also plan to design and install a PG within the soon-to-be-commissioned MMT-POL instrument.

We wish to thank the very useful comments of the anonymous referee that improved this manuscript. C. P. acknowledges National Science Foundation (NSF) support through grant number 0704095. M. J. E. acknowledges NSF support though grant 0621906.

REFERENCES

Adams, J. D., et al. 2006, Proc. SPIE, 6269, 34
Antonucci, R. R. J., & Miller, J. S. 1985, ApJ, 297, 621
Bomzon, Z., Biener, G., Kleiner, V., & Hasman, E. 2001, Opt. Lett., 26, 1711
Broer, D. J., Boven, J., Mol, G. N., & Challa, G. 1989, Makromol. Chem., 190, 2255
Brusa, G., et al. 2003, Proc. SPIE, 4839, 691
Chrysostomou, A., Clark, S. G., Hough, J. H., Gledhill, T. M., McCall, A., & Tamura, M. 1996, MNRAS, 278, 449
Crawford, G. P., Eakin, J. N., Radcliffe, M. D., Callan-Jones, A., & Pelcovits, R. A. 2005, JAP, 98, 123102
Escuti, M. J., Cairns, D. R., & Crawford, G. P 2004, JAP, 95, 5, 2386
Escuti, M. J., & Jones, W. M. 2006, Proc. SPIE, 6332
Escuti, M. J., & Oh, C. 2007, Multi-Layer Achromatic Liquid Crystal Polarization Gratings and Related Fabrication Methods, US Patent 60/912,039 (filed 2008 April 16; issued 2010 September 9)
Escuti, M. J., Oh, C., Sanchez, C., Bastiaansen, C., & Broer, D. J. 2006, Proc. SPIE, 6302, 630207
Fagan, J. A., et al. 2007, Phys. Rev. Lett., 98, 147402
Fox, M. 2001, Optical Properties of Solids (New York: Oxford Univ. Press), 40
Gauza, S., Wang, H., Wen, C.-H., Wu, S.-T., Seed, A. J., & Dabrowski, R. 2003, JaJAP, 42, 3463
Glasse, A. C., Atad-Ettedgui, E. I., & Harris, J. W. 1997, Proc. SPIE, 2871, 1197
Gori, F. 1999, Opt. Lett., 24, 584
Gray, D. E. 1963, American Institute of Physics Handbook (New York: McGraw-Hill)
Hasman, E., Bomzon, Z., Niv, A., Biener, G., & Kleiner, V. 2002, Opt. Commun., 209, 45
Kelly, M. J. 1995, J. Phys. Condensed Matter, 7, 5507
Kim, J., Oh, C., Escuti, M. J., Hosting, L., & Serati, S. 2008, Proc. SPIE, 7093, 709302
Komanduri, R. K., & Escuti, M. J. 2009, Appl. Phys. Lett., 95, 091106
Leroy, J. L. 2000, Polarization of Light and Astronomical Observation (Amsterdam: Gordon Breach)
McManamon, P. F., Bos, P. J., Escuti, M. J., Heikenfeld, J., Serati, S., Xie, H., & Watson, E. A. 2009, Proc. IEEE, 97, 6
Myers, R. M., et al. 2003, Proc. SPIE, 4839, 647
Nersisyan, S. R., Tabiryan, N. V., Steeves, D. M., & Kimball, B. R. 2009, JNOPM, 18, 1
Nikolova, L., & Todorov, T. 1984, AcOpt, 31, 579
Oh, C., & Escuti, M. J. 2006, Opt. Express, 14, 11870
———. 2007, Phys. Rev. A, 76, 4
———. 2007, Proc. SPIE, 6682
———. 2008, Opt. Lett., 33, 2287
Packham, C. C., Axon, D. J., Hough, J. H., Jones, T. J., Roche, P. F., Tamura, M., & Telesco, C. M. 2007, Proc. SPIE, 6678, 66780F
Packham, C., Hough, J. H., & Telesco, C. M. 2005, in ASP Conf. Ser. 343, Astronomical Polarimetry: Current Status and Future Directions (San Francisco: ASP), 38
Packham, C., & Jones, T. J. 2008, Proc. SPIE, 7014, 70145F
Packham, C., Mason, R. E., & Boreman, G. D. 2008, Opt. Eng., 47, 126401
Packham, C., Young, S., Fisher, S., Volk, K., Mason, R., Hough, J. H., Roche, P. F., Elitzur, M., et al. 2007, ApJL, 661, 29
Packham, C., et al. 2008, Proc. SPIE, 7014, 82
Perrin, M. D., Graham, J. R., & Lloyd, J. P. 2008, PASP, 120, 555
Rousset, G., et al. 2003, Proc. SPIE, 4839, 140
Rigaut, F. J., Ellerbroek, B. L., & Flicker, R. 2000, Proc. SPIE, 4007, 1022
Schadt, M., Seiberle, H., & Schuster, A. 1996, Nature, 381, 212
Tamura, M., Fukagawa, M., Kimura, H., Yamamoto, T., Suto, H., & Abe, L. 2006, ApJ, 641, 1172
Tata, R., Martin, E. L., Sengupta, S., Phan-Bao, N., Zapatero Osorio, M. R., & Bouy, H. 2009, A&A, 508, 1423
Tervo, J., & Turunen, J. 2000, Opt. Lett., 25, 785
Wizinowich, P. L., et al. 2000, PASP, Vol. 112, 315
Woollam, J. A., Johs, B. D., Herzinger, C. M., Hilfiker, J. N., Synowicki, R. A., & Bungay, C. L. 1999, Proc. SPIE, CR72, 3